IWSCFF 2022

Formation design of an inter-satellite link demonstration mission

Davide Menzio*, Ahmed Mahfouz†, Florio Dalla Vedova‡, and Holger Voos§

The problem of secular growth of the inter-satellite induced by the J2 perturbations has been widely explored in the literature. In this paper, we study the influence of altitude and initial mean anomaly of the chief on the inter-satellite distance growth in a classical trailing formation. Mean elements are converted into osculating ones and then in Cartesian coordinates that are propagated together in the ECI frame. Preliminary results shows that zonal harmonics are responsible for a steep distance drift when the formation is inserted in the vicinity of ±45 and ±135 degrees of mean anomaly in a polar orbit. Distance-invariant solutions are determined in term of the mean anomaly and characterized in terms of the difference between the average relative distance and the initial one and of the amplitude of the osculating distance. Finally, after the inter-satellite distance has grown to an unacceptable level, the electric thruster onboard of the deputy spacecraft is leveraged in order to reset the deputy's orbit to the distance invariant mean elements. A finite-time Linear Quadratic Regulator (FTLQR) is designed and validated within a high-fidely dynamics framework
keywords: formation design, inter-satellite distance control, perturbations

1. Introduction

Formation flying is a distributed satellite architecture that foresees two or more spacecraft orbiting in a predefined configuration and synchronizing their operations. Combining their instruments results in an improved spatial and temporal sensing ability that could not be achieved with a single satellite. Several applications benefit from this architecture: elevation[17] and cloud[27] profiles mapping, geolocalization,[13] high resolution imagery, gravimetry,[28] and magnetometry,[11] but also, technology demonstrations preparing for active debris removal[12] and on-orbit servicing.[31]

These complex missions could have not been conceived without the efforts of great astrodynamicists. Several models were developed from the Clohessy-Wiltshare[8] to account for different perturbations, induced by an elliptic orbit of the chief satellite[29] or/and the oblateness of the main body.[1,26,32] For Earth-like bodies, the J2 effect induces short-, long-period and secular variations that affect the configuration of the satellites.[7] Schaub and Alfriend noticed that, in first order approximation, the conjugate momenta of the mean elements remains constant while the mean angles grow linearly. With a thoughtful selection of semi-major axis, eccentricity and inclination difference, it is possible to nullify these rates and to bound the motion of the deputy satellites to the chief for few periods.[23] An equivalent reduction of the longitude of the ascending node and the mean argument of the latitude rates can be obtained constraining the along-tracks drift and negating either the differential nodal precession or the differential perigee rotation.[2] Gurfil derived an analytical expression for the inter-satellite distance[14] that was used by Nie to determine conditions for the differential nodal precession (DNPN), the differential periapsis drift (DPRN) and minimum acceleration (MAC).[20] Nie showed that by minimizing the initial drift rate, it is possible to determine solutions in mean elements difference that remain within a 5% margin of the mean inter-satellite distance for about a year. A different approach is the one of Koon et al.,[16] that proposed to initialize the satellite orbits on the center manifold of the periodic orbit that appears in the Routh-reduced system perturbed by zonal harmonics.[6] Nevertheless, upon conversion in osculating elements, the configuration does not survive for more than few days under the effect of the natural drifts. Xu et al. obtained yearly bounded formations by matching the nodal periods and the RAAN drift rates of the pseudo-circular and pseudo-elliptical orbits.[33] Baresi and Scheeres explicitly computed the quasi-periodic invariant tori within the center manifolds of the periodic orbit via a stroboscopic approach and used it to determine trajectories that remain bounded around Earth[4,5] and asteroids.[3] A notable mention is the integrable intermediary of Lara that captures not only secular variations but also short and long period ones.[18] Based on the observation that the analytical solution of the approximation are 1:1 resonant orbit at the critical inclination, Gurfil showed that initializing the chief satellite on a frozen orbit can reduce the inter-satellite dis-

*University of Luxembourg, Luxembourg, Davide.menzio@uni.lu
†University of Luxembourg, Luxembourg, Ahmed.mahfouz@uni.lu
‡LuxSpace Sàrl, Luxembourg, dallavedova@luxspace.lu
§University of Luxembourg, Luxembourg, Holger.voos@uni.lu

tance growth rate.[15]

In this study, a low-thrust system propulsion system is used to control the relative positions in the formation. Indeed, low-thrust systems are different in nature from impulsive thrust ones. For instance, low-thrust systems work in finite time basis and mostly can control not only the direction of the thrust vector, but also its magnitude without having to perform pulse width modulation. This capability made it possible to adopt continuous-time control laws that stem from the classical control theory. Schaub has proposed two Lyaponov-based controllers that are based essentially on the use of the mean orbital elements,[25] while Flack et al. have improved on the low-thrust control laws[9] that had been proposed by Ruggiero.[22]

In this paper, we analyse the effect of the orbital parameters of the chief satellite and different combination of mean elements difference of the deputy on the inters-satellite distance. When it exceeds the limit of 2000 km, the deputy maneuvers to reset its relative orbit and restore its value to 500 km. The reminder of this paper consists of four sections. A brief description of the satellite is given, followed by dynamics, the formation design and the controller design sections. The conclusion is presented in the last section.

2. Triton-X

LuxSpace Sàrl has recently developed Triton-X, a futuristic micro-satellite platform that is planned to reduce the price of earth observation and technology demonstration missions in low earth orbit, without sacrificing power, performance and lifetime. The first mission, for which it is considered, consists in two satellites orbiting an altitude of 450 km above the earth surface. Each satellite is equipped with a radio frequency device allowing the pair to establish the inter-satellite link. The customer required to maintain the relative distance in the 500-2000 km range employing a 7 mN ion thruster.[21]

This work will support LuxSpace Sárl in deploying a two satellite formation performing performing SAR imagery at 450 km altitude relying on inter-satellite link and low-thrust propulsion.

3. Mathematical model

3.1 *Reference frames*

In this paper, two reference frames are used:

- The Earth-Centered Inertial reference frame (ECI) $\mathcal{F}^i$ whose origin is at Earth's center and axes coincide with those of the J2000 frame.
- The Local Vertical Local Horizontal (LVLH) reference frame $\mathcal{F}^l$ which is centered at the satellite's centre of mass with its x-axis pointing away from the center of the Earth, z-axis along the orbit's angular momentum vector, and y-axis completing the right hand triad.

A vector's reference frame is signified using a superscript, either $(\cdot)^i$ or $(\cdot)^l$. However, superscripts are dropped for all the vectors that are represented in the ECI frame to simplify the sequel formulae.

3.2 *Orbital dynamics*

Under the attraction of gravitational field generated by an axial-symmetric body, the gravity potential can be expressed as the sum of a central field and the zonal harmonics terms, as in Eq. 1 :

$$U = \frac{\mu_\oplus}{r}\left[1 - \sum_{j=2}^{4} J_j \left(\frac{R_\oplus}{r}\right)^j P_j(\sin\theta)\right] \qquad [1]$$

where $\mu_\oplus$ is the standard gravitational parameter of the Earth, $R_\oplus$ is the equatorial radius of the Earth, J the zonal harmonic coefficient of j term, reported in Tab. 1, and P the Legendre's polynomial of j degree.

Table 1: Earth zonal coefficients and Legendre's polynomials up to the 4^{th} order

Zonal coefficients		Legendre polynomials	
J_2	1.08262×10^{-3}	P_2	$(3x^2-1)/2$
J_3	-2.5388×10^{-6}	P_3	$(5x^3-3x)/2$
J_4	-1.6560×10^{-6}	P_4	$(35x^4-15x^2+3)/8$

In the presence of an atmosphere, the acceleration of the satellite can be obtained integrating the potential and adding the drag resistance, that can be approximated by Eq. 2:[30]

$$\mathbf{a} = \frac{dU}{dt} - \frac{1}{2}\rho c_D \frac{A}{m} v^2 \frac{\mathbf{v}}{v} + \mathbf{a}_{ctrl} \qquad [2]$$

where ρ is the piece-wise linear atmospheric density measured for high solar and geomagnetic activity,[10] $A/m = 0.25\ m^2/kg$ is the area-to-mass ratio of Triton-X, $C_D = 3.2$ is value of the drag coefficient, and r and v are the Cartesian orbital position and velocity of the satellite in the ECI frame.

The orbit of the chief is modelled in mean elements while the one of the deputy is provided as difference. Let $[a', e', i', \Omega', \omega', M']$ describe the chief state with a the semi-major axis, e the eccentricity, i the inclination, Ω the right ascension of the

ascending node (RAAN), ω the argument of the periapsis, M the mean anomaly, where $'$ indicates the mean elements according to Brouwer's theory.[7] Then $[\delta a', \delta e', \delta i', \delta\Omega', \delta\omega', \delta M']$ denote the mean elements difference of the deputy with δ.

The mean elements are converted, firstly, into osculating ones using the first-order mapping improved by Schaub and Junkins[24] starting from the work of Brouwer[7] and, subsequently, in Cartesian coordinates. as function of the desired initial inter-satellite distance.

Following the work of Gurfil and Lara,[15] a frozen orbit of the deputy is chosen as it shows to reduce the secular drift. For Earth-like planet, the argument of periapsis is fixed at 90 degrees and the eccentricity is defined by the following expression:

$$e = -\frac{J_3}{J_2}\frac{R_\oplus}{2a}\sin i \qquad [3]$$

The inclination is chosen polar while the longitude of the right ascension is fixed to zero for convenience. Despite limited applications, polar orbits are interesting to be studied as they maximize the effect of zonal harmonics in the orbital plane of the satellite.

As it regards the deputy, the choice of its parameters is limited. Given the eccentricity and inclination of the chief, Nie and Gurfil prescribe zero difference in semi-major axis, eccentricity and inclination. This constraint aims at cancelling out the along-track drift and differential nodal precession that are responsible for the secular growth of the inter-satellite distance.[20] In this paper, we consider a classical trailing formation where the difference in longitude of the ascending node and in argument of the periaspsis are not considered and the mean anomaly difference accounts alone for the correct phasing with chief. Its value is computed interpolating the signed distance at the desired level, see Eq. 4:

$$\delta M^* = \text{spline}\left(sign(sin(\delta M))d(\delta M), \delta M, d^*\right) \qquad [4]$$

nwhere d is the inter-satellite distance and $*$ identifies the desired conditions. The sign function ensures that the distance is monotonic and that interpolation is successful. Once the initial conditions for the chief and the deputy have been determined, the Cartesian states of the two satellite are propagated together in the ECI frame. This is possible by resorting the common practice of separating the state in position and velocity. The two sets of ordinary differential equations are integrated with an adaptive step-size Runge-Kutta method that preserves 10^{-9} relative and absolute tolerances. This procedure ensures to retrieve the relative dynamics with a simple subtraction since the states of the two satellites are computed at the same epoch. Moreover, it allows to monitor the evolution of the chief's orbit under the influence of the considered perturbations. In the end, in the case that the chief is equipped with a propulsion system and can be controlled, the dynamics and control of the deputy becomes more complex in an accelerated reference frame and an inertial one is preferred. Although this scenario is not considered in this paper, the TRITON-X platform allows to control both the satellites ,and for this reason, the current formulation of the dynamics was preferred.

The propagation is halted once the inter-satellite distance grows a given value.

4. Formation design

Under these premises, the inter-satellite distance depends only on the initial mean anomaly and the initial altitude of the chief. Therefore a preliminary analysis is conducted to assess how the initial conditions influence the inter-satellite distance evolution in the given dynamics. The analysis is conducted studying the effect of each variable independently, fixing the value of the others and varying the one considered.

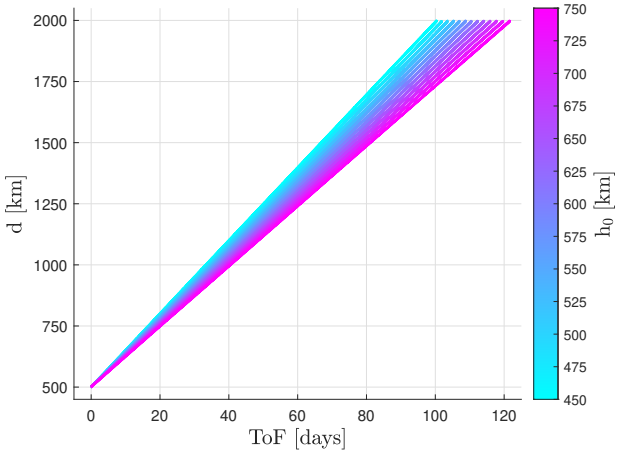

Fig. 1: Inter-satellite distance evolution as function of the initial altitude

Initially the effect of the initial altitude is investigated. Fig. 1 shows how the inter-satellite distance varies initializing the propagation from an altitude changing between 450 and 750 km, that is the operational range considered for the mission. The mean anomaly of the deputy is set to 0 degree, while the one chief is interpolated from the signed distance and varies between 4.201 to 4.024 degrees with the altitude for an initial 500 km of separation.

As expected, the effect of the zonal harmonics is stronger at lower altitude and induces a reduction in the time of free flight during which the formation remains within the 2000 km limit without any control. It passes from 100.359 days to 121.688.

Although a higher altitude is desirable, the customer preferred a lower one, therefore the following analyses employ a 450 km altitude. As seen in the previous section, the mean anomaly of the chief is the only free parameter to study. In this analysis similarly as before, we fix the mean anomaly of the deputy and derive the one of the chief via interpolation. Fig. 2 displays that the distance drift varies significantly with the initial mean anomaly, considering an initial separation of 505 km. This adjustment is beneficial since the zonal harmonics induce a short periodic oscillation of the inter-satellite distance that for large mean anomaly triggers the event function and halts the propagation.

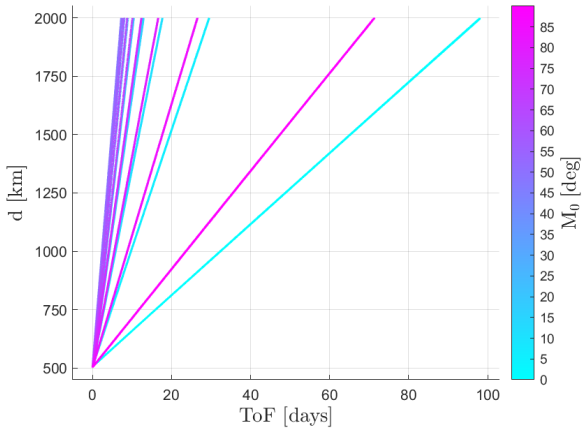

Fig. 2: Inter-satellite distance evolution as function of the initial mean anomaly of the deputy satellite

It is interesting to notice that for the selected values of the mean anomaly, the drift rate is positive and induces the inter-satellite distance to grow secular. Moreover, following the color transition, it can be noticed a shallower trend when the mean anomaly is at the extreme values and gets steeper while moving to the mean value. This behaviour can be easily understood looking at the time of free flight, that varies from 98.014 days obtained for 0 degree of mean anomaly, to 7.260 days for 45 degrees, back to 71.297 days for 85 degrees. In the end, at -5 and 90 degrees the drift rate switches and becomes negative. This insight suggests that for mean anomalies of the 2^{nd} and 4^{th} quadrants the negative drift rate can be leveraged to reduce a large initial separation as it can be seen from Fig. 3.

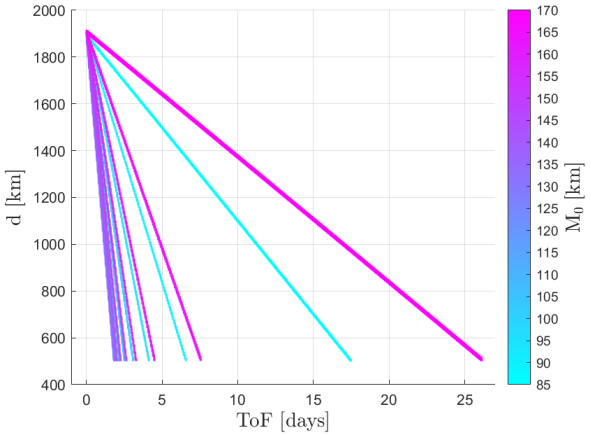

Fig. 3: Inter-satellite distance evolution as function of the initial mean anomaly of the deputy satellite

It is interesting to compare Fig. 2 and Fig. 3. Contrarily to what expected, moving from 500 km of separation to 2000 is not equivalent to the reverse trip. Fig. 3 is more compressed against the y-axis as it can be seen observing that the longest time of free flight measures just 26.125 days.

Finally, since the drift rate change of sign from -5 to 0 degrees and from 85 to 90, a root with zero drift is expected to exist.

4.1 *Invariant inter-satellite distance*

Following this idea, the values of mean anomaly for satellite formation maintaining the initial separation are searched numerically. Combining a grid search approach with an interpolation on the averaged inter-satellite distance, the four invariant solutions represented in Fig. 4 are generated.

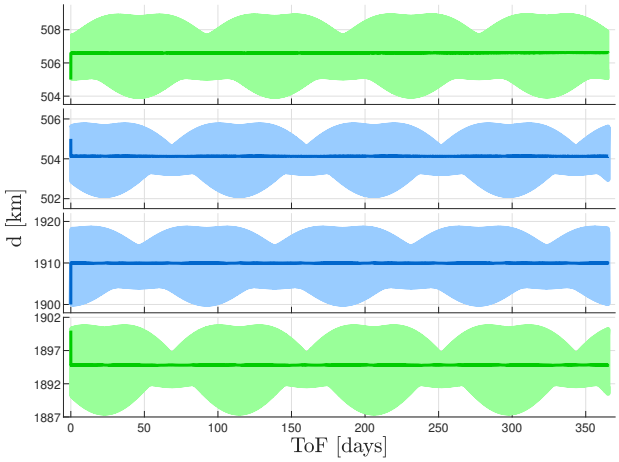

Fig. 4: Invariant inter-satellite distance solutions

The first two solutions are obtained for an initial separation of 505 km and the following sets of mean anomalies for chief and deputy satellites: 2.121 and −2.121 degrees, and 92.150 and 87.912 degrees, respectively. The latter two are computed for an initial separation of 1900 km and the sets of mean anomalies: 187.989 and 172.011, and 98.029 and 82.034 degrees. It is interesting to note that the average mean anomaly of the formation is exactly above the pole, while at the equator, it is offset by few cents of degrees, 0.031 in both cases. Another interesting discovery is the fact that polar initial conditions converge to a plateau in inter-satellite distance that is few km greater than the initial separation: 506.60 km instead of the 505 one at the departure and 1909.95 km instead of the initial 1900. On the other hand, equatorial initial conditions tend to a lower minimum: 504.12 and 1894.8 km, respectively. Conversely, the latter experience smaller variation in osculating distance compared to the former: 4 against 5 km for an initial separation of 505 km and 13 instead of 19 km for the 1900 km case.

These solutions are not practical. They disappear when high fidelity dynamics is considered. For instance, higher order zonal harmonics restore the secular distance drift. Moreover, they are saddle points and small inaccuracy in mean anomaly, few cents of degrees, produce large errors on the terminal inter-satellite distance. The evolution of the inter-satellite distance for the first solution (i.e. with initial separation of 505 km and with a mean anomaly difference of 2.121 degrees) is depicted in Fig. 5.

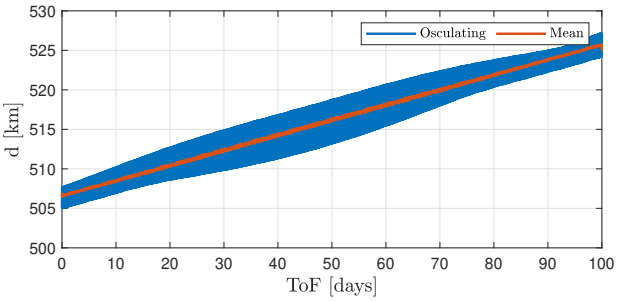

Fig. 5: Evolution of the ISD under high fidelity dynamics for the first solutions

To control the growth of the inter-satellite distance, propulsion system are needed and the following section explains how it is possible to reset your orbit relying on low-thrust propulsion.

5. Control design

Following the discussion in **Section 4**, it is important to note that the change in the inter-satellite distance for the designed formations is accounted for solely by the drift in the mean Argument of Latitude (AoL). All the other differential mean orbital parameters experience almost no change. The drift in the differential mean AoL for the case study of the first solution (see Fig. 5) is depicted in Fig. 6.

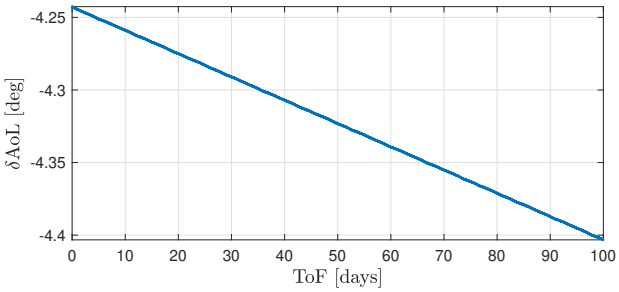

Fig. 6: Evolution of the differential argument of latitude through an uncontrolled propagation

The orbit reset problem in our context concerns only the correction of the AoL of the Deputy spacecraft, and since the chosen orbits for the chief and the deputy are almost circular, the argument of perigee does not have much meaning, and the problem reduces to one in which only the true anomaly needs to be corrected. The problem of orbit reset is hence reformulated as a rendezvous problem between the deputy spacecraft and a hypothetical target point that follows the chief following the constraints which reduce the distance drift (500 km away from the chief). This rendezvous setting is illustrated in Fig. 7. It is important to note that unlike the chief and the deputy, the hypothetical target is propagated using an unperturbed propagator in order to insure that the deputy reaches the required orbital elements no matter after how long. 7.

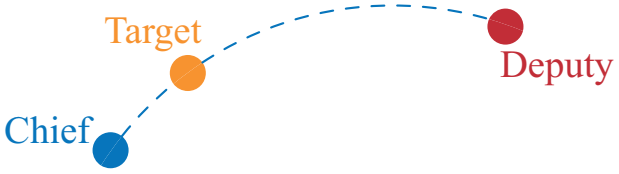

Fig. 7: rendezvous problem formulation

To achieve the rendezvous goal, a simple Finite-Time Linear Quadratic Regulator (FTLQR) controller is adopted. Although LQR is not well known for large rendezvous maneuvers, if a rendezvous between two objects that are drastically far apart is required, the rendezvous between the deputy and the hypothetical target can be subdivided into a handful of sub-rendezvous, each of which is responsible for correcting part of the true anomaly. This idea of sub targets is

illustrated in Fig. 8. For our case study, only about 0.2 degrees of true anomaly (or more precisely argument of latitude) needs to be corrected (see Fig. 6), hence, the sub-division of the rendezvous problem is not necessary.

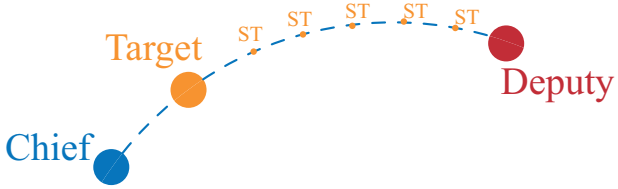

Fig. 8: Sub-targets illustration

5.1 *FTLQR*

The FTLQR scheme is discussed in details by Mathavaraja,[19] nonetheless, a brief discussion is given here for completeness.

The dynamics of the state and the costate vectors are collated and modeled under the LQR scheme as follows:

$$\begin{bmatrix}\dot{\mathbf{x}}^l\\ \dot{\boldsymbol{\lambda}}\end{bmatrix} = \mathbf{A}_a \begin{bmatrix}\mathbf{x}^l\\ \boldsymbol{\lambda}\end{bmatrix},$$
$$\mathbf{A}_a \coloneqq \begin{bmatrix}\mathbf{A} & -\mathbf{B}\mathbf{R}^{-1}\mathbf{B}^\intercal\\ -\mathbf{Q} & -\mathbf{A}^\intercal\end{bmatrix},$$

where $\mathbf{x}^l$ is the baseline vector between the deputy and the instantaneous target, written in the LVLH of the instantaneous target,

$$\mathbf{A} = \frac{\partial \dot{\mathbf{x}}^l}{\partial \mathbf{x}^l}$$

is the Jacobian matrix obtained directly from the Hill-Clohessy-Wiltshire equations,

$$\mathbf{B} = \frac{\partial \dot{\mathbf{x}}^l}{\partial \mathbf{a}^l_{ctrl}}$$

is the control matrix, and $\mathbf{R}$ and $\mathbf{Q}$ are the LQR tunable gains.

For this time invariant system, the State Transition Matrix (STM) between the final and the initial time instants, t_f and t_0, can be written as,

$$\boldsymbol{\Phi}\left(t_f, t_0\right) = \begin{bmatrix}\boldsymbol{\Phi}_{11} & \boldsymbol{\Phi}_{12}\\ \boldsymbol{\Phi}_{21} & \boldsymbol{\Phi}_{22}\end{bmatrix} = e^{\mathbf{A}_a\left(t_f - t_0\right)},$$

where the sub-matrices $\boldsymbol{\Phi}_{11}$, $\boldsymbol{\Phi}_{12}$, $\boldsymbol{\Phi}_{21}$, and $\boldsymbol{\Phi}_{22}$ all have the same dimensions, namely 6×6 for our rendezvous problem.

The FTLQR control acceleration can then be written as,

$$\mathbf{a}^l_{ctrl} = -\mathbf{R}^{-1}\mathbf{B}^\intercal\boldsymbol{\Phi}_{12}^{-1}\left[\mathbf{x}^l\left(t_f\right) - \boldsymbol{\Phi}_{11}\mathbf{x}^l\left(t\right)\right], \quad [5]$$

where t is an arbitrary time instant.

It is important to point out that the final time t_f as well as the final state $\mathbf{x}\left(t_f\right)$ are chosen by the user such that $\left(t_f - t_0\right)$ is the desired time of flight for the maneuver, and $\mathbf{x}\left(t_f\right)$ is the desired final state which is, in effect, a hard terminal constraint. It is conceivably set to zeros for the rendezvous problem. For a perfectly linear time-invariant system with no disturbances or constraints on the actuators, the FTLQR will drive the system from the initial state to the chosen final state within the chosen time window. Indeed, the formation flying system is a nonlinear system which is affected by disturbances that were not taken into account in the FTLQR design process. Moreover, the electric thruster is constrained by the maximum thrust it can produce. Hence, the actual performance of the controller is expected to be degraded even after extensive tuning of the control gains.

5.2 *Actuator model*

The deputy spacecraft is equipped with one electric thruster that can produce a maximum net thrust of T_{max}. It is assumed that the attitude control system is able to reorient the spacecraft in the required thrust direction as quickly and as precisely as the orbit maneuver system requires.

The total thrust vector follows the following dynamics,

$$\hat{\mathbf{T}} = \mathbf{R}^{il}\hat{\mathbf{a}}^l_{ctrl},$$
$$\|\mathbf{T}\| = \begin{cases} T & \text{if } T < T_{max}\\ T_{max} & \text{if } T \geq T_{max}\end{cases},$$
$$T \coloneqq m_d \left\|\mathbf{a}^l_{ctrl}\right\|,$$

where m_d is the instantaneous mass of the deputy spacecraft and $\mathbf{R}^{il}$ is the directional cosine matrix that transforms vectors from the LVLH frame of the instantaneous target to the ECI frame.

5.3 *Controller validation*

The control scheme discussed in *S*ection 5.1 has been validated through numerical simulations for a deputy spacecraft with mass of 200 kg. The simulation results are presented in Fig. 9 for the rendezvous between the deputy and the hypothetical target. The tuned control parameters as well as other simulation settings are summarized in Table 2 in which the subscripts refer to the spacecraft (i.e. $(\cdot)_d$ is a deputy-related quantity and $(\cdot)_t$ is a target-related quantity).

In the presented simulation, the effect of shadow on the performance of the electric thruster is not taken into account.

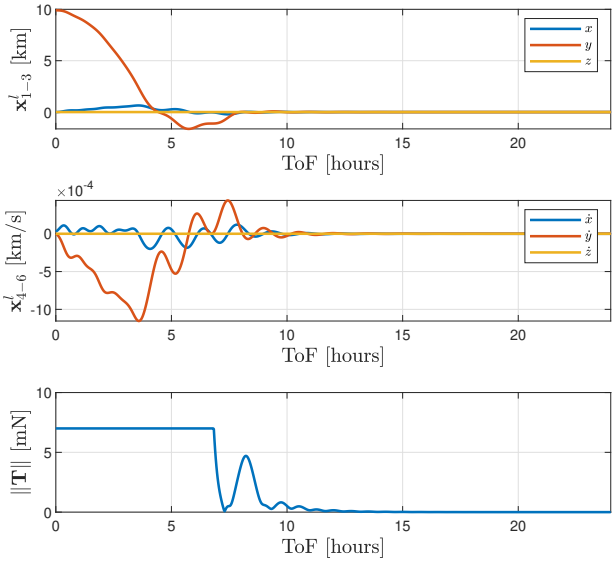

Fig. 9: FTLQR results

t_0	0
t_f	4 hours
$\mathbf{r}_d(0)$	$\begin{bmatrix}-509.54 & 0 & 6809.12\end{bmatrix}^\intercal$km
$\mathbf{v}_d(0)$	$\begin{bmatrix}-7.6191 & 0 & -0.5701\end{bmatrix}^\intercal$km/s
$\mathbf{r}_t(0)$	$\begin{bmatrix}-499.6648 & 0 & 6809.85\end{bmatrix}^\intercal$km
$\mathbf{v}_t(0)$	$\begin{bmatrix}-7.6199 & 0 & -0.5591\end{bmatrix}^\intercal$km/s
$\mathbf{R}$	$10^{10} \times \mathbf{I}_3$
$\mathbf{Q}$	$\begin{bmatrix}10^{-4} \times \mathbf{I}_3 & \mathbf{0}_3 \\ \mathbf{0}_3 & 10^{-2} \times \mathbf{I}_3\end{bmatrix}$
T_{max}	7 mN

Table 2: Simulation settings

Although the time window set for the maneuver is 4 hours, the states did not converge to zero until after 10 hours as seen by Fig. 9, and that is mainly because of the inherent nonlinearities of the formation flying system as well as the nonlinearities that arise from saturating the magnitude of the generated thrust.

6. Conclusion

In this paper, we have analysed the effect initial altitude and the initial mean anomaly on the inter-satellite distance induced by the first three zonal terms. For small initial separation 1^{st} and 3^{rd} quadrants are preferable. Vice-versa, 2^{nd} and 4^{th} for long baselines. Solutions in mean anomaly exist that stabilize the inter-satellite distance growth. For a frozen polar orbit, they are centered either at the pole or at the equator and present a different settling distance and amplitude of the osculating distance. Despite these solutions does not remain distance invariant in high-fidelity dynamics, they are of interest to bound the distance drift. When the inter-satellite distance reaches a predefined threshold, the low-thrust control system is triggered to reset the orbit to its design conditions. A FTLQR control system is implemented and appeared to restore the deputy to its relative initial conditions. Although the adopted control law is mainly suitable for small rendezvous maneuvers between the deputy and a hypothetical target, if the baseline between the deputy and the target is drastically large, the orbit reset problem can be divided into smaller rendezvous problems.

7. Acknowledgement

This work is supported by the Luxembourg National Research Fund (FNR) – AuFoSat project, BRIDGES/19/MS/14302465.

References

[1] K. Alfriend. Nonlinear considerations in satellite formation flying. In *AIAA/AAS Astrodynamics Specialist Conference and Exhibit*, page 4741, 2002.

[2] K. T. Alfriend, S. R. Vadali, P. Gurfil, J. P. How, and L. Breger. *Spacecraft formation flying: Dynamics, control and navigation*, volume 2. Elsevier, 2009.

[3] N. Baresi and D. J. Scheeres. Bounded relative motion under zonal harmonics perturbations. *Celestial Mechanics and Dynamical Astronomy*, 127(4):527–548, 2017.

[4] N. Baresi and D. J. Scheeres. Design of bounded relative trajectories in the earth zonal problem. *Journal of Guidance, Control, and Dynamics*, 40(12):3075–3087, 2017.

[5] N. Baresi, D. J. Scheeres, and H. Schaub. Bounded relative orbits about asteroids for formation flying and applications. *Acta Astronautica*, 123:364–375, 2016.

[6] R. Broucke. Numerical integration of periodic orbits in the main problem of artificial satellite

theory. *Celestial Mechanics and Dynamical Astronomy*, 58(2):99–123, 1994.

[7] D. Brouwer. Solution of the problem of artificial satellite theory without drag. *The Astronomical Journal*, 64:378, nov 1959.

[8] W. Clohessy and R. Wiltshire. Terminal guidance system for satellite rendezvous. *Journal of the Aerospace Sciences*, 27(9):653–658, 1960.

[9] R. D. Falck, W. K. Sjauw, and D. A. Smith. Comparison of low-thrust control laws for applications in planetocentric space. In *50th AIAA/ASME/SAE/ASEE Joint Propulsion Conference*, page 3714, 2014.

[10] E. C. for Space Standardization. Space environment ecss-e-st-10-04c. Technical report, 2019. Rev. 1.

[11] E. Friis-Christensen, H. Lühr, and G. Hulot. Swarm: A constellation to study the earth's magnetic field. *Earth, planets and space*, 58(4):351–358, 2006.

[12] E. Gill, S. D'Amico, and O. Montenbruck. Autonomous formation flying for the prisma mission. *Journal of Spacecraft and Rockets*, 44(3):671–681, 2007.

[13] P. Gurfil, J. Herscovitz, and M. Pariente. The samson project–cluster flight and geolocation with three autonomous nano-satellites. 2012.

[14] P. Gurfil and K. V. Kholshevnikov. Manifolds and metrics in the relative spacecraft motion problem. *Journal of guidance, control, and dynamics*, 29(4):1004–1010, 2006.

[15] P. Gurfil and M. Lara. Motion near frozen orbits as a means for mitigating satellite relative drift. *Celestial Mechanics and Dynamical Astronomy*, 116(3):213–227, 2013.

[16] W. Koon, J. Marsden, R. Murray, and J. Masdemont. J2 dynamics and formation flight. In *AIAA Guidance, Navigation, and Control Conference and Exhibit*, page 4090, 2001.

[17] R. Kroes, O. Montenbruck, W. Bertiger, and P. Visser. Precise grace baseline determination using gps. *Gps Solutions*, 9(1):21–31, 2005.

[18] M. Lara and P. Gurfil. Integrable approximation of j 2-perturbed relative orbits. *Celestial Mechanics and Dynamical Astronomy*, 114(3):229–254, 2012.

[19] S. Mathavaraj and R. Padhi. *Satellite Formation Flying: High Precision Guidance Using Optimal and Adaptive Control Techniques*. Springer Nature, 2021.

[20] T. Nie, P. Gurfil, and S. Zhang. Analytical conditions for bounded mean inter-satellite distances in the j 2 problem. *Journal of Guidance, Control, and Dynamics*, 41(10):2144–2162, 2018.

[21] OHB LuxSpace. *TRITON-X The high-performance microsatellite platform*.

[22] A. Ruggiero, P. Pergola, S. Marcuccio, and M. Andrenucci. Low-thrust maneuvers for the efficient correction of orbital elements. In *32nd International Electric Propulsion Conference*, pages 11–15, 2011.

[23] H. Schaub and K. T. Alfriend. J2 invariant relative orbits for spacecraft formations. *Celestial Mechanics and Dynamical Astronomy*, 79(2):77–95, 2001.

[24] H. Schaub and J. L. Junkins. *Analytical mechanics of space systems*. AIAA Education Series, 2009.

[25] H. Schaub, S. R. Vadali, J. L. Junkins, and K. T. Alfriend. Spacecraft formation flying control using mean orbit elements. *The Journal of the Astronautical Sciences*, 48(1):69–87, 2000.

[26] S. A. Schweighart and R. J. Sedwick. High-fidelity linearized j model for satellite formation flight. *Journal of Guidance, Control, and Dynamics*, 25(6):1073–1080, 2002.

[27] G. L. Stephens, D. G. Vane, R. J. Boain, G. G. Mace, K. Sassen, Z. Wang, A. J. Illingworth, E. J. O'connor, W. B. Rossow, S. L. Durden, et al. The cloudsat mission and the a-train: A new dimension of space-based observations of clouds and precipitation. *Bulletin of the American Meteorological Society*, 83(12):1771–1790, 2002.

[28] B. D. Tapley, S. Bettadpur, M. Watkins, and C. Reigber. The gravity recovery and climate experiment: Mission overview and early results. *Geophysical research letters*, 31(9), 2004.

[29] J. Tschauner and P. Hempel. Rendezvous zu einem in elliptischer bahn umlaufenden ziel. *Astronautica Acta*, 11(2):104–+, 1965.

[30] D. A. Vallado. *Fundamentals of astrodynamics and applications*, volume 12. Springer Science & Business Media, 2001.

[31] D. A. Whelan, E. A. Adler, S. B. Wilson III, and G. M. Roesler Jr. Darpa orbital express program: Effecting a revolution in space-based systems. In *Small Payloads in Space*, volume 4136, pages 48–56. SPIE, 2000.

[32] G. Xu and D. Wang. Nonlinear dynamic equations of satellite relative motion around an oblate earth. *Journal of Guidance, Control, and Dynamics*, 31(5):1521–1524, 2008.

[33] M. Xu, Y. Wang, and S. Xu. On the existence of j 2 invariant relative orbits from the dynamical system point of view. *Celestial Mechanics and Dynamical Astronomy*, 112(4):427–444, 2012.

View publication stats